

# Applied Magnetic Field Rejects the Coating of Ferromagnetic Carbon from the Surface of Ferromagnetic Cobalt: RAPET of $\text{CoZr}_2(\text{acac})_2(\text{O}^i\text{Pr})_8$

Vilas G. Pol,<sup>†</sup> Swati V. Pol,<sup>†</sup> Aharon Gedanken,<sup>\*,†</sup> Vadim G. Kessler,<sup>‡</sup> Gulaim A. Seisenbaeva,<sup>‡</sup> Mun-Gyu Sung,<sup>§</sup> and Shigeo Asai<sup>§</sup>

Department of Chemistry and Kanbar Laboratory for Nanomaterials at the Bar-Ilan University Center for Advanced Materials and Nanotechnology, Bar-Ilan University, Ramat-Gan, 52900, Israel, Department of Chemistry, SLU, Box 7015, 75007 Uppsala, Sweden, and Department of Materials Processing Engineering, Graduate School of Engineering, Nagoya University, Furo-cho, Chikusa-ku, Nagoya 464-8603, Japan

Received: November 30, 2004; In Final Form: February 8, 2005

We present the results of the RAPET (reaction under autogenic pressure at elevated temperatures) dissociation of  $\text{CoZr}_2(\text{acac})_2(\text{O}^i\text{Pr})_8$  at 700 °C in a closed Swagelok cell under an applied magnetic field of 10 T. It produces a mixture of carbon-coated and noncoated metastable  $\text{ZrO}_2$  nanoparticles, bare metallic Co nanoparticles, and bare carbon. The same reaction in the absence of a magnetic field produces spherical Co and  $\text{ZrO}_2$  particles in sizes ranging from 11 to 16 nm and exhibiting, at room temperature, metastable phases: fcc for cobalt and a tetragonal phase for zirconia. The metastable phases of Co and  $\text{ZrO}_2$  are manifested because of a carbon shell of ~4 nm thickness anchored to their surfaces. The effect of an applied magnetic field to synthesize morphologically different, but structurally the same, products is the key topic of the present paper.

## Introduction

Zirconia ( $\text{ZrO}_2$ ) is a remarkable material that has attracted a great deal of attention from scientists, technologists, and industrial users. Zirconia has three crystal structures, namely, monoclinic, tetragonal, and cubic. The physical and chemical properties of zirconia are closely related to its different crystal phases and determine its application in industry.<sup>1</sup> The mechanical, chemical, and catalytic properties of zirconia can be improved by using nanocrystalline instead of conventional micron-sized zirconia. Various groups have employed a range of wet-chemistry methods to synthesize Co– $\text{ZrO}_2$  catalyst.<sup>2–6</sup> However, complicated apparatus, complex process controls, and special conditions are required for these approaches.

RAPET (Reaction under Autogenic Pressure at Elevated Temperatures), which uses a single precursor process, has recently been designed for the fabrication of nanomaterials. A simple, one-step, solvent- and catalyst-free RAPET reaction, which does not use any stabilizing agent, was developed to fabricate metastable fcc Co and tetragonal  $\text{ZrO}_2$  phases. The RAPET synthesis of these metastable structures was reported in our previous publication.<sup>7</sup> The stabilization of metastable fcc cobalt and the tetragonal phase of zirconia can be seen due to an in situ formed carbon shell of ~4 nm thickness. The current investigation, centered on the decomposition of a  $\text{CoZr}_2(\text{acac})_2(\text{O}^i\text{Pr})_8$  in a closed cell at 700 °C, was conducted under the application of a high magnetic field of 10 T. To the best of our knowledge, there are no previous reports on the effect of applying a magnetic field on the rejection of ferromagnetic carbon from the surface of cobalt particles. This article shows how the magnetic field affects the morphology of the products of this reaction, which in the absence of a magnetic field leads

to the formation of carbon-coated  $\text{ZrO}_2$  and Co nanoparticles. The application of the magnetic field of 10 T leads to the formation of carbon-coated metastable  $\text{ZrO}_2$  (~5%) and noncoated  $\text{ZrO}_2$  (95%) nanoparticles, as well as separated carbon structures. By selected area energy-dispersive X-ray analysis (SAEDS), a trace amount of Co (~6 wt %) was found in 95% of the  $\text{ZrO}_2$  which was not covered by carbon. It is interesting to understand the reason for the removal of the carbon shell from the surface of  $\text{ZrO}_2$  nanoparticles. We have recently reported on the effect of a magnetic field on a RAPET of  $\text{MoO}(\text{OMe})_4$ .<sup>8</sup> The decomposition of molybdenum oxymethoxide in a magnetic field has led to the fabrication of  $\text{MoO}_2$  nanoparticles and separated carbon particles.<sup>8</sup> The magnetic field-guided formation of long carbon filaments (sausages) is also reported.<sup>9</sup> The RAPET product of the present reaction (applied magnetic field) is characterized by structural, morphological, and magnetic properties and is compared with the reaction that was carried out without a magnetic field. The changes in the morphology are attributed to the effect of the applied magnetic field.

## Experimental Section

The fabrication of Co and  $\text{ZrO}_2$  nanoparticles separately coated with carbon via RAPET reaction is discussed elsewhere.<sup>7</sup> The obtained composite was termed a carbon-coated cobalt/zirconia nanocomposite (CCZN) sample. The same procedure was carried out under a static magnetic field of 10 T, which was generated using a helium-free superconducting magnet. The Swagelok cell was set in the maximum magnetic point in the bore of the magnet, where the gradient of the magnetic field was the smallest. A ceramic oven containing the Swagelok cell filled with 0.5 g of  $\text{CoZr}_2(\text{acac})_2(\text{O}^i\text{Pr})_8$  was placed between the poles of the magnetic field. The oven was heated and cooled at the same rates used for the reaction without a magnetic field. The total yield of product material was about 63% of the total weight of  $\text{CoZr}_2(\text{acac})_2(\text{O}^i\text{Pr})_8$  introduced in the cell (the yield is the final weight of the product relative to the weight of the

\* Corresponding author. E-mail: gedanken@mail.biu.ac.il.

<sup>†</sup> Bar-Ilan University.

<sup>‡</sup> SLU.

<sup>§</sup> Nagoya University.

starting material). This is termed a zirconia–cobalt prepared under magnetic field (ZCPMF) sample. The yields obtained in the reaction carried out with and without the magnetic field were approximately the same.

We termed this new method for the synthesis of various nanomaterials RAPET (Reaction under Autogenic Pressure at Elevated Temperatures). Using this method, we have prepared uniform, monodispersed carbon spherules,<sup>10</sup> nanosized Si coated carbon spheres,<sup>11</sup> and core–shell structures of metals/metal oxides with carbon from various alkoxides.<sup>12</sup> The present RAPET method for the synthesis of nanomaterials requires simple equipment, comparatively low temperature, and a short reaction time, and it produces pure products.

### Characterization

The ZCPMF composite is characterized by various techniques. (X-ray diffraction (XRD) patterns were collected by using a Bruker AXS D\* Advance powder X-ray diffractometer (Cu K $\alpha$  radiation, wavelength 1.5406 Å). The morphologies and nanostructure of the as-synthesized products were further characterized with a JEM-1200EX transmission electron microscopy (TEM) model and a JEOL-2010 high-resolution TEM (HR-TEM) model using accelerating voltages of 80 and 200 kV, respectively. SAEDS (selected-area energy-dispersive X-ray analysis) of one individual particle was conducted using a JEOL-2010 HR-TEM model and energy-dispersive X-ray analysis (EDX) by using an X-ray microanalyzer (Oxford Scientific), both attached to a JSM-840 scanning electron microscope (SEM). Samples for TEM and HR-TEM were prepared by ultrasonically dispersing the products into absolute ethanol, placing a drop of this suspension onto a copper grid coated with an amorphous carbon film, and then drying in air. A Scion image software program was used to measure the mean particle size of ZrO<sub>2</sub> nanoparticles. The elemental analysis of the samples was carried out by an Eager 200 C, H, N, S analyzer. The Olympus BX41 (Jobin Yvon Horiba) Raman spectrometer was employed, using the 514.5 nm line of an Ar laser as the excitation source to analyze the nature of the carbon present in the ZCPMF material. The magnetic measurements of ZCPMF material were performed on a Vibrating Sample Magnetometer (VSM-Oxford-3001).

### Results and Discussion

Elemental (C, H, N, S) and energy-dispersive X-ray analysis (EDX) are briefly described here since they are almost the same as that reported in the previous article.<sup>7</sup> The measured element percentage of carbon in the ZCPMF product is 9.12% ( $\sim 0.0261$  g), while the percentage of hydrogen is 0.06%. The presence of zirconium, cobalt, carbon, and oxygen in the ZCPMF material was examined by EDX measurement. The EDX spectrum was also used to obtain a quantitative estimate of the Zr and Co. For the light elements such as oxygen and carbon, only a rough estimate could be obtained. In the ZCPMF product the weight ratio of Zr:Co is 3.5:1, while the calculated ratio in the starting materials is 3.1:1.

The morphology of the ZCPMF sample was studied by low-resolution TEM (LR-TEM), and the structure was studied by HR-TEM and XRD measurements. The LR-TEM picture shown in Figure 1a illustrates that most of the particles are not surrounded by any contrasting material; i.e., they are noncoated. Only after a very careful observation is it found that (Figure 1b) very few spherical particles are coated with a nanolayer of a material having a different contrast. The ratio of these carbon-coated particles to noncoated particles is 5:95. This ratio was

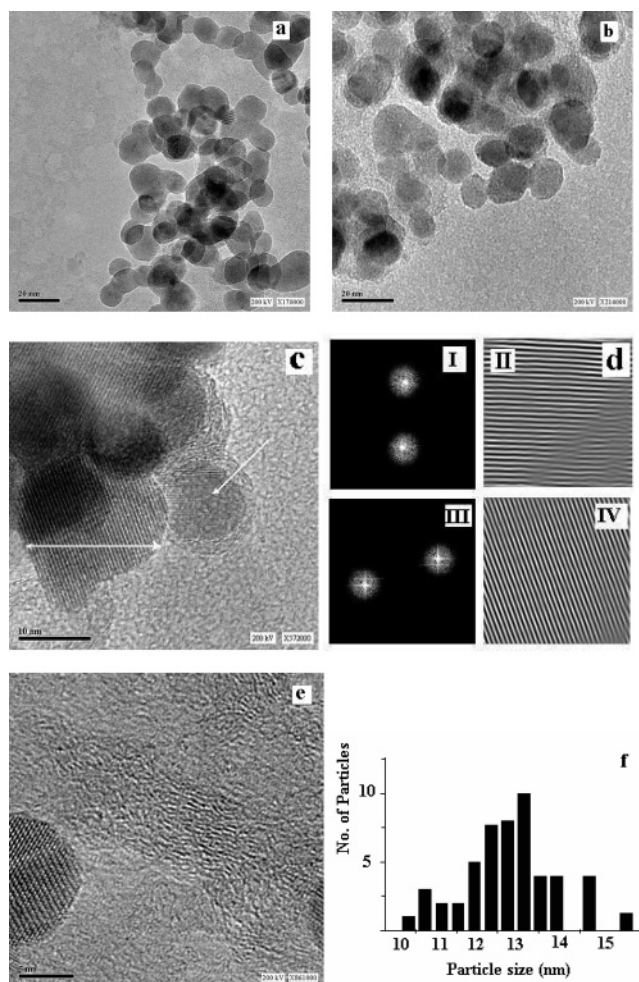


**Figure 1.** Pictures of (a) LR-TEM of ZCPMF sample; (b) HR-TEM of ZCPMF sample; (c) HR-TEM of ZCPMF sample; (d) the masked fast Fourier transform (FFT) image (I) and its inverse FFT (II) depicted from (c) (CCZ particle) and the masked fast Fourier transform (FFT) image (III) and its inverse FFT (IV) depicted from (c) (ZNC particle); (e) noncoated carbon sheets/layers shown at HR; and (f) statistical particle size analysis of the histogram obtained from the TEM in (a).

found from the LR-TEM picture using a Scion image software program. In contrast, all the Co/ZrO<sub>2</sub> particles were found to be carbon coated in the CCZN sample. This indicates that the carbon shell is removed from the products, which are prepared under a magnetic field.

The HR-TEM of (marked by an arrow) a carbon-coated (5%) zirconia particle is depicted in Figure 1c. The picture provides evidence for the existence of the tetragonal ZrO<sub>2</sub> core. It illustrates the perfect arrangement of the atomic layers and the lack of defects. The measured distance between these (101) lattice planes is 0.299 nm, which is very close to the distance between the planes reported in the literature (0.295 nm) for the tetragonal phase of the ZrO<sub>2</sub> (PDF: 79-1770). Since such carbon-coated particles are  $\sim 5\%$  in the ZCPMF product, we termed them carbon coated zirconia (CCZ) particles. The other particle shown in Figure 1c (double-sided arrow) is not covered with carbon, and different interlayer spacings, 0.256 nm, are measured. These spacings are related to the (002) lattice planes of metastable tetragonal zirconia. As already explained,  $\sim 95\%$  of the ZrO<sub>2</sub> particles are not carbon coated, and we termed them zirconia noncoated by carbon (ZNC) particles. The question that arises is if both particles in Figure 1c are zirconia, then why one of them is coated with carbon while the other is not? To

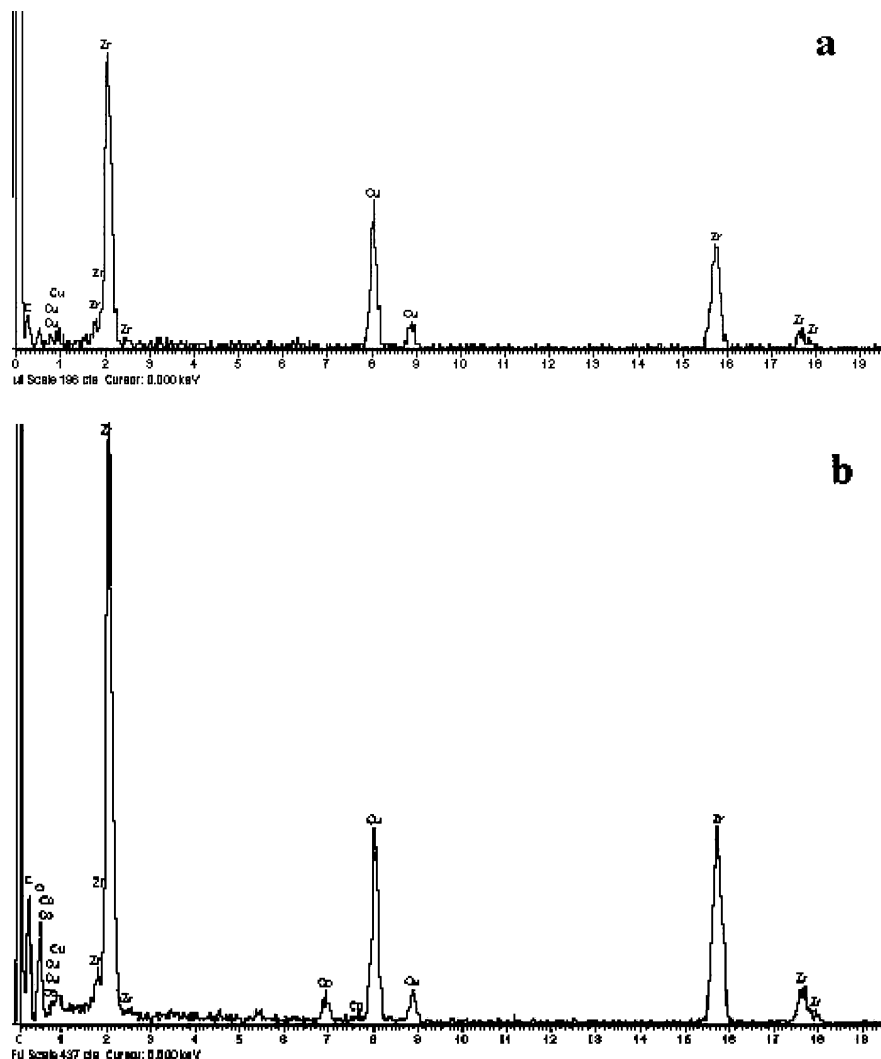


**Figure 2.** SAEDS analysis of CCZ particle (a) and ZNC particle (b).

further substantiate our identification of the ZNC and CCZ particles, SAEDS measurements were performed.

The typical SAEDS presented in Figure 2a for a CCZ particle shows the presence of Zr, O, C, and Cu. From this observation, it is clear that the particles that are coated with carbon (CCZ) are of pure  $\text{ZrO}_2$ , lacking the presence of cobalt. However, the typical SAEDS presented in Figure 2b shows the presence of a small amount of Co and large amounts of Zr, O, C, and Cu for the ZNC particle. The weight percent of cobalt with  $\text{ZrO}_2$  is  $\sim 6:94$ . We have focused a 25 nm electron beam on the center of the several particles to understand the composition. It was observed that most of the particles are  $\text{ZrO}_2$  rich and have a trace amount of cobalt. This proves that there are two types of zirconia particles present in the nanocomposite: carbon-coated particles that do not contain cobalt and uncoated particles that have a trace amount of cobalt. It is logical that the particles possessing a small amount of cobalt are responsible for removing/rejecting the carbon from the surface of the zirconia during the application of the magnetic field. We have not detected any particles rich with cobalt in the SAEDS analysis. The bulk EDX analysis of the ZCPMF product shows that the weight percentages of Co and Zr are 22% and 78%, respectively. However, by SAEDS analysis for the ZCPMF sample, the weight percent of Co with Zr is 6% and 94%. There is clearly some more cobalt that is not detected in the SAEDS. This loss of cobalt can be explained as follows. Some of the bare ferromagnetic Co particles might have formed agglomerates,

which did not reach the TEM grid, but were detected by EDX. That is why the weight percentage of Co measured by bulk EDX and SAEDS is not the same. We conclude that the RAPET dissociation of  $\text{CoZr}_2(\text{acac})_2(\text{O}^i\text{Pr})_8$  at 700 °C under an applied magnetic field of 10 T yielded Co,  $\text{ZrO}_2$  particles possessing trace cobalt, and  $\text{ZrO}_2$  particles. From XRD measurements, the presence of  $\text{ZrO}_2$  and Co is observed in their metastable phases, namely, tetragonal for zirconia and fcc for cobalt (see XRD paragraph). Figure 1d represents the masked fast Fourier transform (FFT) image (I) and its inverse FFT (II) depicted from Figure 1c of CCZ particle and the masked fast Fourier transform (FFT) image (III) and its inverse FFT (IV) depicted from Figure 1c of ZNC particle.

Disordered and ordered carbon layers were formed during the magnetic rejection of carbon from the cobalt surfaces, as detected by Raman spectroscopy (see below). The interlayer spacing of the carbon layers is  $\sim 0.35$  nm, very close to the distance between the graphitic layers (Figure 1e). A statistical analysis of the histogram obtained from the TEM picture (Figure 1a) shows that the mean size of the core of  $\text{ZrO}_2$  nanoparticles is  $13.6 \pm 0.3$  nm. The histogram reveals (Figure 1f) a size distribution of the particles in the range of 10–16 nm.

The mechanism that is proposed for the effect of the applied magnetic field is as follows. The magnetic field affects the morphology of the present reaction product, which in the absence of a magnetic field leads to the formation of carbon-coated  $\text{ZrO}_2$  and Co nanoparticles.<sup>7</sup> It is believed that the small

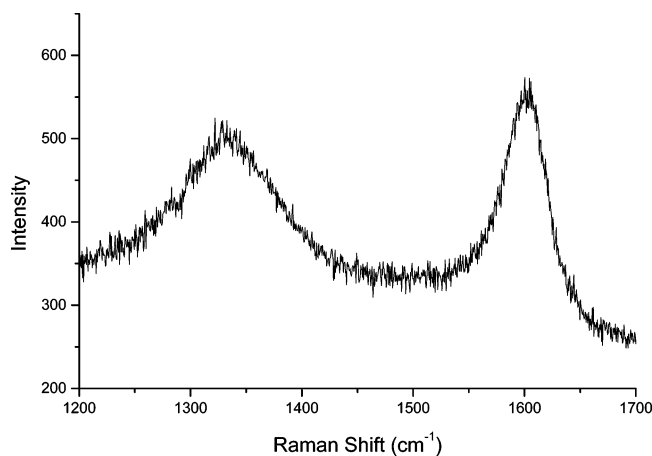


**Figure 3.** Raman spectrum of ZCPMF sample.

amount of cobalt atoms in CCZ ( $\text{ZrO}_2(\text{tetragonal})/\text{C}$ ), observed in the SAEDS, is responsible for the rejection of carbon from the particle's surface. Cobalt is well known as a catalyst for the growth of carbon around it, and indeed, in the absence of a magnetic field a carbon shell is formed<sup>7</sup> around the  $\text{ZrO}_2/\text{Co}$  core. Under a magnetic field about 95% of the  $\text{ZrO}_2$  particles possess cobalt, and no carbon coating is obtained. The reason for the removal of the carbon shell from the surface of  $\text{ZrO}_2$  nanoparticles is the rejection due to magnetic forces between the trace amount of Co and the approaching carbon particles. A similar rejection process has occurred in the  $\text{MoO}_2$  experiments.<sup>8</sup> However, the difference there is in the amount and nature of the core. The core in the previous case was 100%  $\text{MoO}_2$ , while in the current studies the same rejection is caused by 6% cobalt. This is due to the ferromagnetic (Co) versus paramagnetic ( $\text{MoO}_2$ ) nature of the relative cores. The RAPET of 1,3,5-trimethylbenzene ( $\text{C}_6\text{H}_3(\text{CH}_3)_3$ ) also showed the magnetic field effects on the product morphology, which without the magnetic field leads to the formation of uniform, monodispersed, high-purity carbon spherules (CSs) without using a catalyst.<sup>10</sup> The magnetic field induced the interaction between the stable radicals and caused the growth of the carbon body to form long (up to 32  $\mu\text{m}$ ) carbon filaments/sausages.<sup>9</sup>

Whether magnetic carbon exists<sup>13</sup> or not, the suggested structure of the ferromagnetic carbon (equal number of  $\text{sp}^2$  and  $\text{sp}^3$  hybridized carbon atoms) was studied by Ovchinnikov et al. and Shamovsky.<sup>14</sup> Since the ZCPMF product contains a 9.12% element of carbon, Raman spectroscopic measurements were performed to understand the nature of the carbon. The micro-Raman spectrum of ZCPMF sample is shown in Figure 3. The two characteristic bands of carbon were detected at  $1345 \text{ cm}^{-1}$  (D-band) and  $1598 \text{ cm}^{-1}$  (G-band). The intensity of the G-band, associated with graphitic carbon, is larger than the intensity of the D-band.<sup>15</sup> The intensity ratio of the D- and G-bands is  $I_D/I_G = 0.8$  for the ZCPMF sample. According to our assumption, the precursor is completely dissociated at  $700 \text{ }^\circ\text{C}$  to carbon and hydrogen atoms. We speculate that perhaps the carbon formed upon this dissociation is ferromagnetic, and its strong interaction with the ferromagnetic Co or even paramagnetic  $\text{MoO}_2$  leads to its rejection from the surface of the substrate. Upon cooling, the ZCPMF product fabricated in a magnetic field at  $700 \text{ }^\circ\text{C}/3 \text{ h}$  causes the formation of Co and  $\text{ZrO}_2$  with a trace amount of Co particles, which solidifies first, to reject any approaching ferromagnetic carbon moiety. The 5% of the zirconia particles that lack the cobalt presence are carbon coated. The 95% zirconia particles that contain traces of cobalt

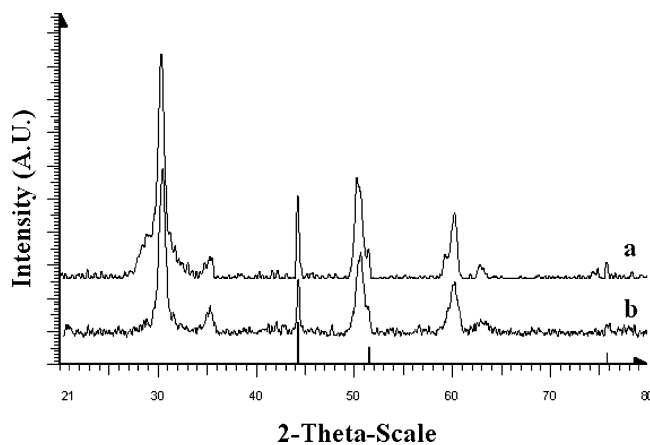


**Figure 4.** Powder XRD patterns of (a) CCZN sample and (b) ZCPMF sample.

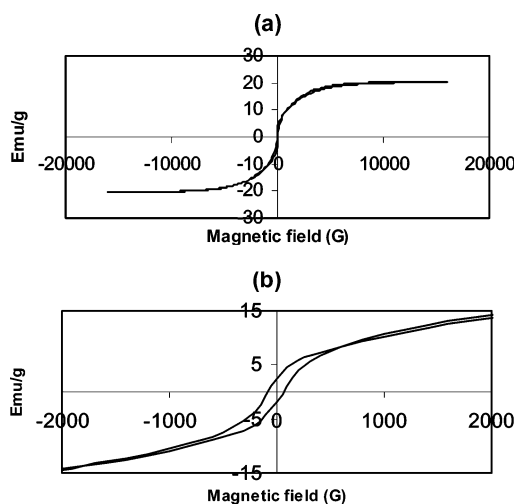


**Figure 5.** Magnetization vs magnetic field curves for ZCPMF sample: (a) complete hysteresis loop and (b) same plot enlarged for coercivity ( $H_c$ ) and remanent magnetization ( $M_r$ ) observation.

further confirm our arguments regarding the magnetic rejection between ferromagnetic cobalt and carbon.

The remaining question is why are the  $\text{ZrO}_2$  particles formed in the metastable tetragonal phase even without the carbon shell? The tetragonal phase is unchanged even after aging for a long time (a few months) at ambient conditions, as evidenced from the XRD patterns in Figure 4. Our explanation is the particle-size effect: the as-formed  $\text{ZrO}_2$  particles are  $\sim 10\text{--}16 \text{ nm}$ , as observed by TEM measurements. The critical size is 6 nm, as reported in the literature,<sup>16</sup> for the stabilization of a 100% tetragonal phase of zirconia.<sup>16</sup> More recently, Shukla et al. demonstrated the aggregation tendency<sup>17</sup> of  $\sim 45 \text{ nm}$  zirconia, which is responsible for the stabilizing metastable tetragonal phase, within large ( $\sim 500\text{--}600 \text{ nm}$ ) undoped zirconia particles. We therefore attribute the stability of the tetragonal phase to the size effect. This is reinforced by the presence of a trace amount of cobalt, which might effect the stabilization of the metastable tetragonal phase of zirconia.

The XRD patterns of the CCZN and ZCPMF samples are presented in Figure 4. The major peaks and their intensities at  $2\theta$  values of  $30.24$ ,  $50.25$ ,  $60.24$ , and  $62.89^\circ$  correspond to the reflection lines of the metastable tetragonal phase of zirconia. These values are in good agreement with the diffraction peaks, peak intensity, and cell parameters of crystalline  $\text{ZrO}_2$  (PDF No. 79-1770). The peak widths for the metastable tetragonal phase of zirconia, at full width at half-maxima (fwhm), are wide,

indicating a small crystallite size ( $\sim 14$  nm) for both cases. The indicated diffraction lines at  $2\theta$  values of  $44.2$  and  $51.47^\circ$  are assigned to the crystalline face centered cubic phase of cobalt (PDF No. 15-806). Almost the same XRD patterns, with no characteristic peaks of carbon, were observed for the CCZN and ZCPMF samples, and this might be due to the amorphous nature of carbon. XRD measurements for CCZN and ZCPMF samples after a few months at ambient conditions did not detect any change in the diffraction peaks, thus confirming the stability of metastable phases.

The magnetic properties of the ZCPMF sample were investigated by magnetic susceptibility measurements, as outlined in the Experimental Section. The magnetization vs magnetic field curve for the ZCPMF sample shows a ferromagnetic<sup>18</sup> behavior (Figure 5). The values for the saturation magnetization ( $M_s$ ), coercivity ( $H_c$ ), and remanent magnetization ( $M_r$ ) are  $20 \text{ emu g}^{-1}$ ,  $70 \text{ Oe}$ , and  $2.5 \text{ emu g}^{-1}$ , respectively, for the ZCPMF sample. Taking into account the weight of the cobalt present throughout the material (by EDX), the saturation magnetization is  $91 \text{ emu g}^{-1}$  in the ZCPMF sample.

**Acknowledgment.** V.G.P. and S.V.P. are grateful to Bar-Ilan University, Israel, for financial assistance.

### References and Notes

- (1) Shukla, S.; Seal, S.; Vij, R.; Bandyopadhyay, S. *Nano Lett.* **2003**, *3*, 397.
- (2) Lick, I. D.; Carrascull, A.; Ponzi, M.; Ponzi, E. N. *Catal. Lett.* **2003**, *89*, 179.
- (3) Orlik, S. N.; Struzhko, V. L.; Mironyuk, T. V.; Tel'biz, G. M. *Kinet. Catal.* **2003**, *44*, 682.
- (4) Stefanov, P.; Atanasova, G.; Marinova, T.; Gomez-Garcia, J.; Sanz, J.; Caballero, M. A.; Morales, J. J.; Cordon, A. M.; Gonzalez-Elipse, A. R. *Catal. Lett.* **2003**, *90*, 195.
- (5) Hattink, B. J.; Labarta, A.; del Muro M. G.; Batlle, X.; Sanchez, F.; Varela, M. *Phys. Rev. B* **2003**, *67*, 033402.
- (6) Ohnuma, S.; Lee, H. J.; Kobayashi, N.; Fujimori, H.; Masumoto, T. *IEEE Trans. Magn.* **2001**, *37*, 2251.
- (7) Pol, S. V.; Pol, V. G.; Seisenbaeva, G.; Kessler, V. G.; Gedanken, A. *Chem. Mater.* **2004**, *16*, 1793.
- (8) Pol, S. V.; Pol, V. G.; Kessler, V. G.; Seisenbaeva, G. A.; Sung, M.; Asai, S.; Gedanken, A. *J. Phys. Chem B* **2004**, *108*, 6322.
- (9) Pol, V. G.; Pol, S. V.; Gedanken, A.; Sung, M.; Asai, S. *Carbon* **2004**, *13*, 2738.
- (10) Pol, V. G.; Motiei, M.; Gedanken, A.; Calderon-Moreno, J.; Yoshimura, M. *Carbon* **2004**, *42*, 111.
- (11) Pol, V. G.; Pol, S. V.; Gedanken, A.; Goffer, Y. *J. Mater. Chem.* **2004**, *14*, 966.
- (12) Pol, S. V.; Pol, V. G.; Gedanken, A. *Chem.—Eur. J.* **2004**, *10*, 4467.
- (13) Makarova, T. L.; Sundqvist, B.; Hohne, R.; Esquinazi, P.; Kopelevich, Y.; Scharff, P.; Davydov, V. A.; Kashevarova, L. S.; Rakhmanina, A. V. *Nature* **2001**, *413*, 716.
- (14) Ovchinnikov, A. A.; Shamovsky, I. L. *THEOCHEM—J. Mol. Struct.* **1991**, *83*, 133.
- (15) Dresselhaus, M. S.; Dresselhaus, G.; Pimenta, M. A.; Eklund, P. C. In *Analytical Application of Raman Spectroscopy*; Pelletier, M. J., Ed.; Blackwell Science: Oxford, 1999; Chapter 9.
- (16) Nitsche, R.; Winterer, M.; Hahn, H. *Nanostruct. Mater.* **1995**, *6*, 679.
- (17) Shukla, S.; Seal, S.; Vij, R.; Bandyopadhyay, S.; Rahman, Z. *Nano Lett.* **2002**, *2*, 989.
- (18) Liu, S. W.; Zhu, J. J.; Mastai, Y.; Felner, I.; Gedanken, A. *Chem. Mater.* **2000**, *12*, 2205.